Biogerontology (2018) 19:223–235
https://doi.org/10.1007/s10522-018-9751-y

RESEARCH ARTICLE

Involvement of the autophagic pathway in the progression of AMD-like retinopathy in senescence-accelerated OXYS rats

Oyuna S. Kozhevnikova · Darya V. Telegina · Vasiliy A. Devyatkin · Nataliya G. Kolosova

Received: 17 January 2018 / Accepted: 24 February 2018 / Published online: 28 February 2018

Abstract Age-related macular degeneration (AMD) is a complex neurodegenerative disease resulting in a loss of central vision in the elderly. It is currently assumed that impairment of autophagy may be one of the key mechanisms leading to AMD. Here we estimated the influence of age-related autophagy alterations in the retina on the development of AMD-like retinopathy in senescence-accelerated OXYS rats. Significant changes in the expression of the autophagy proteins were absent at the age preceding the development of retinopathy (age 20 days). We found increased levels of LC3A/B, Atg7, and Atg12–Atg5 conjugated proteins in the OXYS retina during manifestation of this retinopathy at the age of 3 months. By contrast, in the retina of 18-month-old OXYS rats with a progressive stage of retinopathy, we revealed significantly decreased protein levels of Atg7 and Atg12–Atg5 as compared to age-matched Wistar rats. Simultaneously with perturbation of the autophagic response, the necrosome subunits Ripk1 and Ripk3 were detected in the OXYS retina. The downregulation of autophagy markers coincided with amyloid β accumulation (Moab-2) in the retinal pigment epithelium and choroid. Using high-throughput RNA sequencing, we found a missense single-nucleotide polymorphism (SNP) in the *Pik3c2b* gene associated with autophagy regulation. This SNP was predicted to significantly affect protein structure. Our data prove participation of the autophagic pathway in the progression of AMD-like retinopathy.

Keywords Aging · Senescence-accelerated OXYS rats · Age-related macular degeneration · Autophagy · *Pik3c2b*

O. S. Kozhevnikova (✉) · D. V. Telegina · V. A. Devyatkin · N. G. Kolosova
Institute of Cytology and Genetics, SB RAS, Novosibirsk, Russia
e-mail: oidopova@bionet.nsc.ru

V. A. Devyatkin · N. G. Kolosova
Novosibirsk State University, Novosibirsk, Russia

Introduction

Age-related macular degeneration (AMD) is a complex neurodegenerative progressive eye disease, resulting in severe loss of central vision in the aging population. The AMD morbidity rate is growing as part of the trend toward aging of the general population in developed countries. Despite the high prevalence of AMD, to date, there is no treatment of dry AMD. A major obstacle for good understanding of the pathophysiology of AMD is its complexity and the lack of a single animal model that can fully replicate key features of the human disease. This situation is primarily due to the multifactorial origin of AMD, such as human genetic polymorphisms and long-term exposure to environmental factors that induce epigenetic changes (Lim et al. 2012). Development of AMD

is based on age-associated changes of retinal pigment epithelium (RPE), Bruch's membrane, and choriocapillaris, but the exact mechanisms initiating the transition from typical age-related changes to the pathological process remain poorly understood. Currently, it is postulated that oxidative stress and a chronic aberrant inflammatory response in RPE cells are the main pathological factors that drive AMD (Lim et al. 2012).

There is a growing body of evidence suggesting that impairment of autophagy may be one of the key mechanisms leading to AMD (Mitter et al. 2014; Zhang et al. 2015; Golestaneh et al. 2017; Kaarniranta et al. 2017). Autophagy is an evolutionarily conserved cellular housekeeping process that removes damaged organelles and protein aggregates that are dysfunctional or unnecessary to the cells by delivering cytoplasmic substrates to lysosomes for degradation (Zhang et al. 2015). Compromised autophagy has been implicated in many neurodegenerative diseases, including retinal degeneration. By modulating cellular metabolism and quality control, autophagy thus stands at the crossroads between survival and cell death, as stated by K. Kaarniranta et al. (2017). Autophagy impairments result in homeostasis dysregulation, accumulation of dysfunctional and toxic proteins, damaged organelles, and lipofuscin and formation of precipitates of AMD-specific drusen, thereby promoting inflammation. Autophagy impairment is considered a potential therapeutic target for AMD prevention; however, the mechanisms behind age-dependent autophagy dysregulation in the retina and their contribution to the AMD pathogenesis and progression remain obscure. Because in humans, the research on the pathogenesis of AMD, especially early asymptomatic stages is problematic, there is a need for animal models that closely mirror the human pathology.

There is evidence that a suitable experimental model of AMD is senescence-accelerated OXYS rats, which spontaneously develop a phenotype similar to human age-related disorders including AMD-like retinopathy (Kozhevnikova et al. 2013a, b; Muraleva et al. 2014; Stefanova et al. 2014; Telegina et al. 2015, 2017a). Retinopathy that develops in OXYS rats already at a young age corresponds (in terms of clinical manifestations and morphological characteristics) to the dry atrophic form of AMD in humans. Nonetheless, neovascularization develops in some ($\sim$ 10–20%) of these rats with age. The clinical signs of AMD-like retinopathy appear by the age of 3 months in 100% of OXYS rats against the background of a reduction in the transverse area of the RPE, impairment of choroidal microcirculation, and retinal thinning (Muraleva et al. 2014). The progression of these abnormalities in OXYS rats until the age of 10 months is accompanied by a significant reduction in thickness of the photoreceptor cell layer and a reduction in the number of photoreceptor cell nuclei of the outer nuclear layer, especially in the central part of the retina (Korbolina et al. 2016). Significant pathological changes in the RPE manifest themselves as excessive accumulation of lipofuscin and amyloid in the RPE regions (Kozhevnikova et al. 2013b), disturbances in the morphology of the RPE sheet, including an increase in the proportion of multinucleated cells, hypertrophy, distortion of cell shape, and reactive gliosis (Telegina et al. 2017a).

Our recent study showed a modest role of apoptosis at advanced stages of retinopathy in OXYS rats despite the altered expression profile of cell death genes (Telegina et al. 2015), pointing to preferential involvement of other types of cell death in the retina during AMD (Telegina et al. 2017b). We hypothesized that the autophagic pathway is involved in neuronal retinal degeneration in OXYS rats. Therefore, the aim of this study was to assess the age-related changes of autophagy in the retina of OXYS and control Wistar rats and contributions of autophagy to the development of AMD-like pathology in OXYS rats, including the preclinical stage. We found a deficiency in the development of the autophagy response in OXYS rats with age, in contrast to control rats. This problem probably caused amyloid β (Aβ) accumulation and activation of necroptosis. Using previously obtained high-throughput RNA sequencing (RNA-seq) data, we identified a missense single-nucleotide polymorphism (SNP) in the *Pik3c2b* gene associated with autophagy regulation. This SNP was predicted to significantly affect protein structure (scored as "deleterious") by the Variant Effect Predictor tool, VEP (SIFT algorithm) and has not been described in Ensemble. Here we provide evidence for altered autophagic function in the pathophysiology of AMD-like retinopathy in the OXYS rat model.

Methods

Animals

Male senescence-accelerated OXYS rats at preclinical (20 days), early (3 months), and late (18 months) stages of the disease (8 per group) and age-matched male Wistar rats (as controls) were obtained from the Breeding Experimental Animal Laboratory of the Institute of Cytology and Genetics, the Siberian Branch of the Russian Academy of Sciences (Novosibirsk, Russia). The study did not include females because of the possible influence of the hormonal background on the process of autophagy. For immunohistochemical analysis, three rats were randomly selected from each age group. At least four tissue slices were analyzed per animal. For western blot analysis, five rats were randomly selected from each age group. The OXYS rat strain was derived from the Wistar rat strain at the Institute of Cytology and Genetics as described earlier (Kolosova et al. 2014) and was registered in the Rat Genome Database (http://rgd.mcw.edu/). At this point, we have the 109th generation of OXYS rats with spontaneously developing accelerated senescence syndrome including AMD-like retinopathy inherited in a linked manner.

All the animal procedures and experimental protocols were approved by the Institutional Review Board of the Institute of Cytology and Genetics, according to The Guidelines for Manipulations of Experimental Animals. At age 4 weeks, the pups were weaned, housed in groups of five animals per cage (57 × 36 × 20 cm), and kept under standard laboratory conditions (22 °C ± 2 °C, 60% relative humidity, 12 h light/12 h dark cycle; lights on at 9 a.m.). The rats were provided with standard rodent feed (PK-120-1, Ltd., Laboratorsnab, Russia) and given water ad libitum.

Antibodies

Rabbit recombinant monoclonal anti-Atg7 (ab133528), rabbit polyclonal anti-Atg12 (ab155589), goat polyclonal anti-Iba1 (ab5076), rabbit polyclonal anti-Ripk1 (ab106393, Abcam), rabbit polyclonal anti-Ripk3 (ab62344), rabbit polyclonal anti-LC3A/B (ab128025), mouse monoclonal anti-β-actin [AC-15] (ab6276), donkey anti-mouse IgG H&L (conjugated with Alexa Fluor® 568; ab175472), donkey anti-goat IgG H&L (conjugated with Alexa Fluor® 488; ab150129), goat anti-rabbit IgG H&L preadsorbed (conjugated with Alexa Fluor® 488; ab150081), goat anti-rabbit IgG H&L (conjugated with horseradish peroxidase [HRP]; ab6721), and sheep anti-mouse IgG H&L antibodies (HRP; ab6808) were acquired from Abcam. A mouse monoclonal anti–amyloid β peptide antibody (MOAB-2; MABN254) was purchased from Millipore.

RPE-choroid flat-mount staining

Rats were euthanized by CO_2 asphyxiation; after decapitation, the eyes were excised and fixed in 4% paraformaldehyde in phosphate-buffered saline (PBS; 0.01 M, pH 7.4) for 2 h. After a wash in PBS, the eyes were cryoprotected in graded sucrose solutions (10, 20, and 30%). The eyes were enucleated, and the anterior segment and retina were removed. The remaining RPE–choroid complex was embedded in Killik (Bio-Optica), frozen, and stored at −80 °C. The RPE–choroid complex was thoroughly washed, permeabilized with 1% Triton X-100 in PBS and incubated for 1 h with a blocking solution (5% bovine serum albumin, 0.3% Triton X-100 in PBS). Primary antibodies, i.e., the mouse monoclonal anti–amyloid β peptide antibody (MOAB-2; MABN254, Millipore, 1:100) and goat polyclonal anti-Iba1 antibody (ab5076, 1:100, Abcam) were incubated with the tissue slices overnight at 4 °C. Secondary antibodies, i.e., the donkey anti-goat IgG H&L antibody (conjugated with Alexa Fluor® 488; ab150129, Abcam, 1:200) and donkey anti-mouse IgG H&L antibody (conjugated with Alexa Fluor® 568; ab175472, Abcam, 1:200) were applied to the slices, with incubation for 2 h at room temperature. After thorough washes, the slices were flat-mounted on glass slides and were coverslipped with the Fluoro-shield mounting medium containing 4′,6-diamidino-2-phenylindole (DAPI; ab104139, Abcam). Images were acquired with a confocal microscope (LSM 780 NLO, Zeiss).

Immunohistochemistry

The eyes were removed and fixed in fresh 4% paraformaldehyde in PBS for 2 h, washed three times in PBS, and then cryoprotected in graded sucrose solutions (10, 20, and 30%). Posterior eyecups were

embedded in Killik (Bio-Optica), frozen, and stored at −80 °C. Tissue slices (10 μm thick) were prepared on a Microm HM-505 N cryostat at –20 °C, transferred onto Polysine® glass slides (Menzel-Glaser), and stored at −20 °C. The slices were incubated for 1 h in 5% BSA with 0.1% Triton X-100 in PBS, followed by overnight incubation at 4 °C with the rabbit antibodies to LC3A/B Atg7 (1:150 dilution, ab133528), to Atg12 (1:150 dilution, ab155589), to Ripk1 (1:100 dilution, ab106393), and to Ripk3 (1:100 dilution, ab62344). After several washes in PBS, the tissue slices were incubated with the secondary antibody conjugated with Alexa Fluor® 488 (ab150081) at a dilution of 1:100 for 2 h and subsequently washed with PBS. The slices were coverslipped with the Fluoroshield mounting medium supplemented with DAPI (Abcam) and were examined under the microscope Axioplan 2 (Zeiss). Images for LC3A/B were acquired by means of the confocal microscope (LSM 780 NLO, Zeiss). The negative control samples with the omitted primary antibody emitted only a minimal autofluorescent signal. For each image acquisition, all imaging parameters were the same.

Administration of propidium iodide (PI) and detection of PI-positive cells

Propidium iodide (PI) is a nucleic acid stain. Once the dye is bound to nucleic acids, its fluorescence increases 20- to 30-fold. Because PI cannot penetrate the plasma membrane, it is also used to detect necrotic cells (Unal Cevik and Dalkara 2003). When the cell membrane is disrupted, PI leaks into the cell and binds to DNA and RNA and, therefore, only necrotic cells fluoresce red. PI (10 mg/mL; Sigma) was diluted in 0.9% NaCl, and at 1 mg/kg was administered 2 h before killing by intraperitoneal injection to 12-month-old Wistar and OXYS rats (n = 3). The eyes were collected and fixed in fresh 4% paraformaldehyde in PBS for 2 h, washed three times in PBS, and then cryoprotected in graded sucrose solutions (10, 20, and 30%). Posterior eyecups were embedded in Killik (Bio-Optica), frozen, and stored at −80 °C. The cryostat-made slices (10 μm thick) were placed on Polysine® glass slides (Menzel-Glaser) cover-slipped with the Fluoroshield mounting medium containing with DAPI (Abcam), and were examined under the fluorescence microscope Axioplan 2 (Zeiss) with excitation/emission filters at 568/585 nm for PI.

Western blotting

Immunoblotting was performed as previously described (Muraleva et al. 2014). Antibodies and dilutions in this study included anti-Atg7 (1:2000), anti-Atg12 (1:1000), and anti-β-actin antibodies (1:2000). After blockage with 5% bovine serum albumin in PBS with 0.1% Tween 20 for 1 h, the membranes were incubated with the primary antibodies at 4 °C overnight. After incubation with the secondary antibody (1:3000), chemiluminescent signals were measured and scanned, and intensity of the bands was quantified in the ImageJ software. β-Actin always served as an internal loading control.

SNP discovery in previously obtained RNA-seq data

Illumina sequencing data were analyzed previously as described by Telegina et al. (2015). Briefly, over 40 million single-end reads of 50-bp length were obtained per sample (in triplicate for OXYS and Wistar rats) of retinal RNAs, by Illumina nonstranded sequencing (on an Illumina GA IIx in the "Genoanalitika" Lab) in accordance with standard Illumina protocols (mRNA-Seq Sample Prep Kit). After barcode trimming, the sequencing data were tested for quality in the FastQC software and mapped to the *Rattus norvegicus* reference genome assembly RGSC 5.0 (Ensemble release 75) by means of Bowtie 2 or TopHat v2.0.4. The SNP positions within the aligned reads relative to the reference genome were identified using the pileup function in SAM tools (v. 0.1.17) utilities. Via various filter commands, SNPs were predicted for various positions with a minimum mapping quality (Q) of 100. These parameters ensure high-quality, reliable mapping of the reads, which is important for variant calling. We verified that each mutation was present in all OXYS rats and was not present in any of the Wistar rats using custom-designed Java scripts. The effect of a variant amino acid substitution on protein function was predicted by the Variant Effect Predictor Web service (http://www.ensembl.org/); the consequence type, SIFT score, and prediction were obtained for each variant. Generally, SIFT scores of 0–0.05 were

classified as "deleterious" and 0.05–1.00 as "tolerated."

Sanger sequencing

For verification purposes, we carried out Sanger sequencing of the gene region containing the deleterious SNPs in genomic DNA obtained from liver samples of different OXYS rats. Matrix enrichment and Sanger reactions were conducted using the oligonucleotide 5′-TCCACTTACGATTCGGAGAT-3′ as the forward primer and 5′-CTGCCTCCCATAATAAAGCC-3′ as the reverse one.

Statistical analysis

The data were subjected to analysis of variance (ANOVA in the Statistica 8.0 software). The post hoc test was applied to significant main effects and interactions to assess the differences between some sets of means. The data are shown as mean ± SEM. The differences were considered statistically significant at $p < 0.05$.

Results

Age-related alterations of Atg7 and Atg12 expression in the rat retina

Atg7 and Atg12 are required components of the autophagosome maturation pathway. Western blot analysis and immunohistochemistry were undertaken to determine age-related changes in their expression in the retina among 20-day-old and 3- and 18-month-old OXYS and Wistar rats (Fig. 1).

The western blotting revealed that the amount of protein Atg7 was not affected by age or genotype. We found no significant change in the levels of Atg7 with age in OXYS rats, while in Wistar rats, this parameter increased only by 18 months of age ($p < 0.05$). Nevertheless, the Atg7 expression increased in 3-month-old OXYS rats ($p < 0.05$), but this level decreased at age 18 months as compared to Wistar rats ($p < 0.05$; Fig. 1a, c).

The western blotting data were confirmed by immunohistochemical analysis. Analysis of the results of immunohistochemical staining of the retinal slices showed that Atg7 expression dominated in the inner plexiform layer (IPL) and ganglion cell layer (GCL) of rats of both strains and all ages (Fig. 1d). We did not detect significant changes in the expression of the Atg7 protein between OXYS and Wistar rats at age 20 days. The content of Atg7 in the retina of OXYS rats increased by age 3 months in GCL and became higher than that in Wistar rats. By the age of 18 months, the amount of Atg7 decreased in the retina of the OXYS strain to the level of 20-day-old rats. On the contrary, in the Wistar retina, the expression of Atg7 increased in GCL until the age of 18 months.

To further evaluate the alterations of the autophagy during accelerated retina aging in OXYS rats, we analyzed the amounts of the Atg5–Atg12 conjugated complex in the two rat strains. Western blotting revealed that the amount of Atg5–Atg12 conjugated complex was not affected by age and genotype. Content of the Atg5−Atg12 conjugated complex in the retina of Wistar rats increased by age 18 months ($p < 0.05$), while in OXYS rats, these parameters did not change with age. We found significantly decreased levels of the Atg5–Atg12 conjugated complex in 18-month-old OXYS rats ($p < 0.05$) as compared to Wistar rats (Fig. 1b, c).

The immunostaining of retinal cryosections revealed that Atg12 was present distinctly at the level of inner segments of the photoreceptor layer and in the photoreceptors themselves (ONL). In the other retinal layers, Atg12 immunofluorescence was weaker and showed a tendency to increase with age. No obvious difference was seen in Atg12 immunostaining between Wistar and OXYS rats at the ages of 20 days and 3 months. At the age of 18 months, we noticed a well-pronounced reduction of Atg12 labeling in OXYS retina (Fig. 1e). Notably, the observed reduction in autophagy markers in the retinas of the old OXYS rats was accompanied by a reduced number of photoreceptor cells in the ONL.

Age-related alterations of LC3A/B immunostaining in the rat retina

We measured LC3A/B levels by fluorescence microscopy in retinal sections from 20-day-old and 3- and 18-month-old OXYS and Wistar rats. Diffuse weak LC3A/B staining was observed in all retinal layers of 20-day-old rats of both strains. With age, expression of LC3A/B increased in both rat strains. By the age of 3 months in OXYS rats in contrast to Wistar rats,

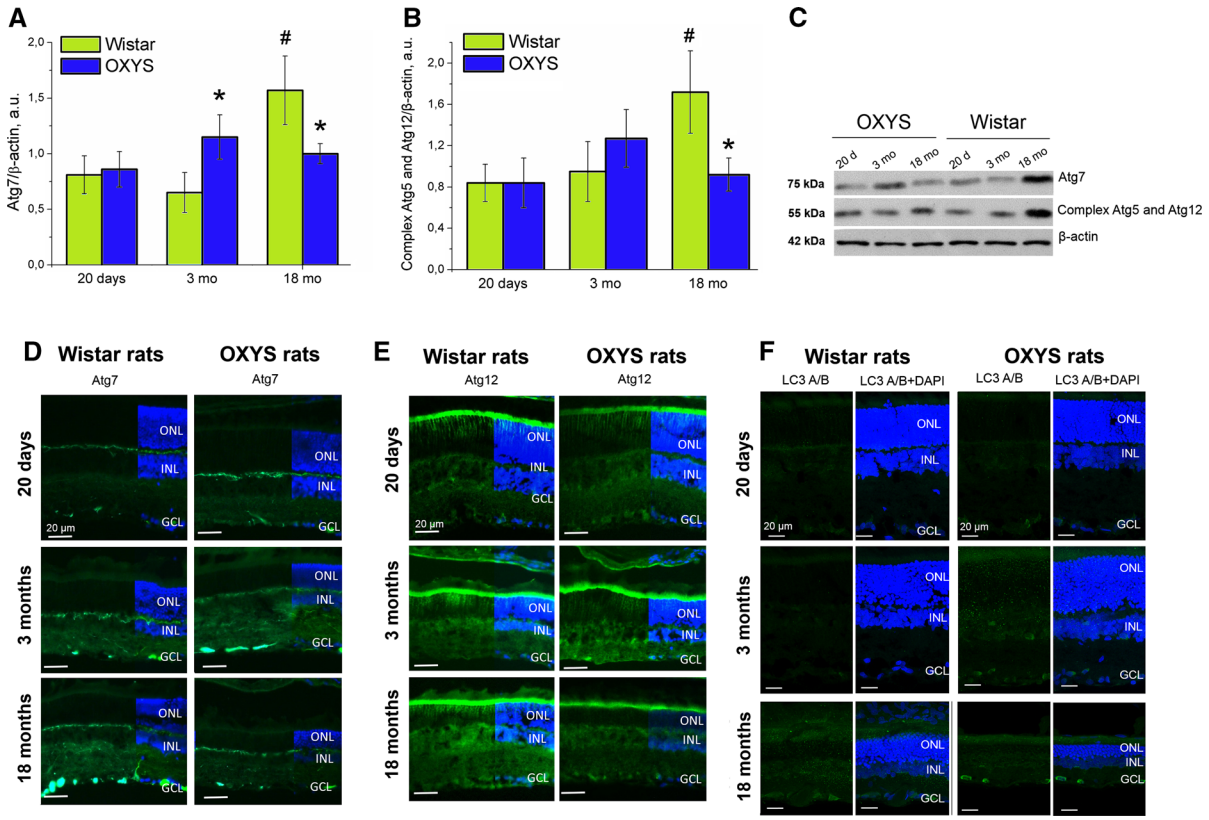

Fig. 1 Expression of the Atg7 protein in retinas from normal Wistar rats and from OXYS rats with AMD-like retinopathy. **a** Levels of the Atg7 protein in retinal homogenates from Wistar and OXYS rats. **b** Amounts of the Atg5–Atg12 conjugate complex in retinal homogenates from Wistar and OXYS rats. **c** Representative immunoblots of Atg7 and of the Atg5–Atg12 conjugate complex in the retina of OXYS and Wistar rats. Representative immunofluorescent images of retinal cryosections from 20-day-old and 3- and 18-month-old OXYS and Wistar rats. Retinas were fixed in paraformaldehyde, cryoprotected, cut, and immunostained for Atg7 (**d**), Atg12 (**e**), and LC3A/B (**f**), and DAPI was applied to visualize the nuclei. Data are presented as mean ± SEM, *Interstrain differences, ^age-associated differences; $p < 0.05$. ONL: outer nuclear layer, INL: inner nuclear layer, GCL: ganglion cell layer. Scale bar: 20 μm

LC3A/B labeling appeared as numerous fluorescent dots with strong immunoreactivity in neurons' somas of some cells of GCL and INL. At the age of 18 months, Wistar rats also manifested a significant increase in LC3A/B puncta in all retinal layers, slightly more intense than in age-matched OXYS rats. Although LC3A/B labeling of some individual ganglion neurons increased in 18-month-old OXYS rats, the overall retinal number of LC3A/B puncta decreased as compared to 3 months (Fig. 1f). This result may indicate a decrease of autophagosome formation in the aged OXYS retina, and the unsuccessful packaging of waste material for autophagic degradation.

Localization of necrosome subunits Ripk1 and Ripk3 in the rat retina

Necrosis was found to be a regulated process mediated by receptor-interacting protein kinases (RIPKs) (Trichonas et al. 2010). The localization of proteins Ripk1 and Ripk3 in the retina, which are necessary for initiation of programmed necrosis (Dvoriantchikova et al. 2014), was evaluated by immunohistochemistry. Ripk1-specific immunostaining was present in the photoreceptor inner/outer segment layer in OXYS and Wistar rats of all ages. In the GCL of OXYS rats, Ripk1 immunostaining was evident at ages 3 and 18 months, but in Wistar rats' GCL, Ripk1 immunostaining was detected only at the age of 18 months (Fig. 2a). Immunofluorescence of Ripk3 was present

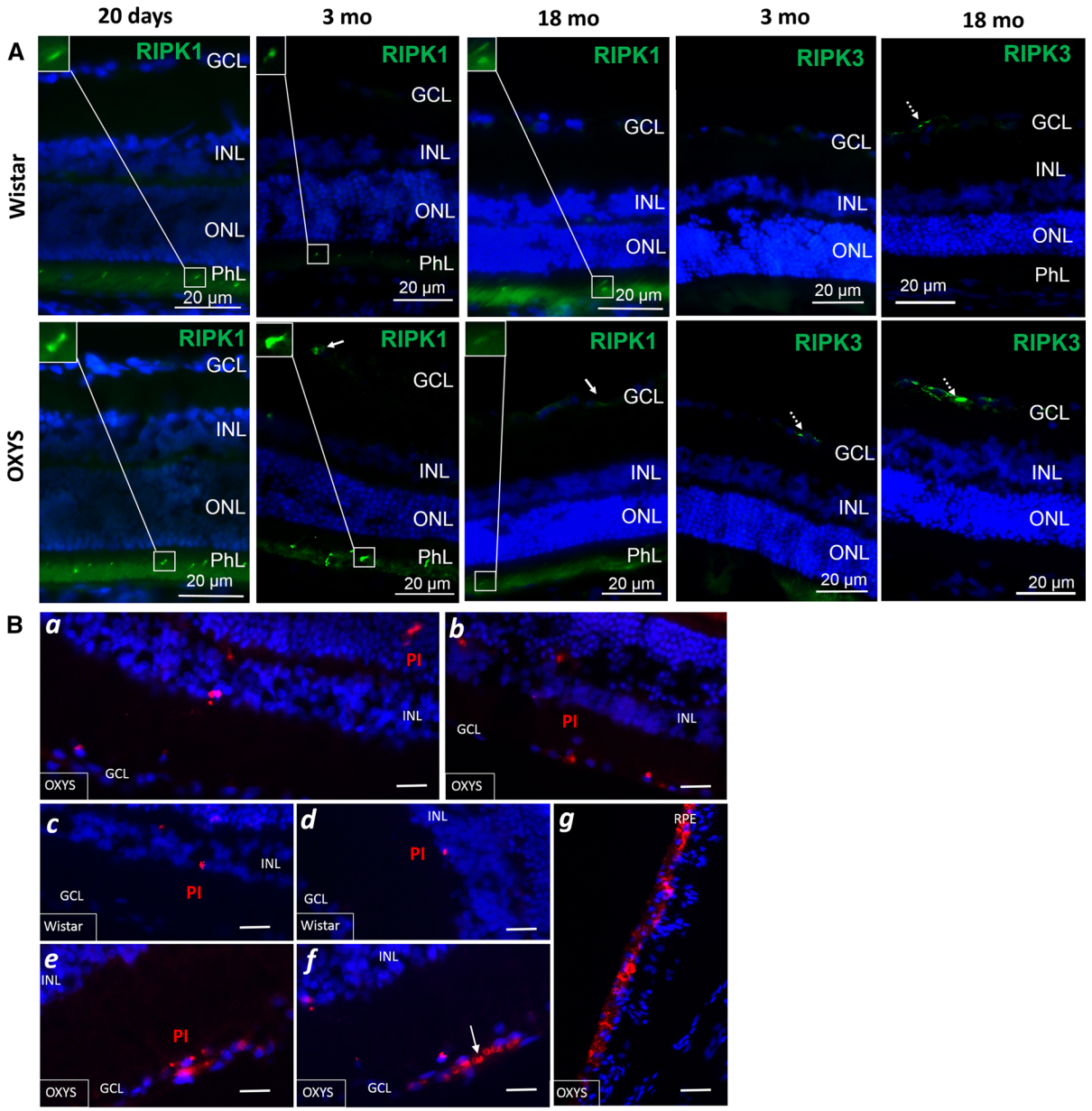

Fig. 2 Markers of necroptosis. **A** Representative images of retinal cryosections immunostained by Ripk1 and Ripk3, from 20-day- and 3- and 18-month-old OXYS and Wistar rats. Arrows and inserts depict inclusions of Ripk1 in PhL. Dotted arrows indicate signals of Ripk3 in GCL. **B** Examples of propidium iodide (PI) fluorescence in the retina after in vivo administration to the OXYS (*a, b, e, f*) and Wistar retina (*c, d*). Injection of PI increased autofluorescence of erythrocytes (*f*) and RPE cells (*g*). DAPI was used to visualize the nuclei. *ONL* outer nuclear layer, *INL* inner nuclear layer, *GCL* ganglion cell layer, *PhL* outer segments of photoreceptors, *RPE* retinal pigment epithelium, *PI* propidium iodide. Scale bar: 20 μm

in the GCL of OXYS rats starting from the age of 3 months. In the GCL of Wistar rats, it was found only at the age of 18 month (Fig. 2b).

PI fluorescence in the rat retina

Plasmalemma permeability is a hallmark of necrotic, including necroptotic, cell death (You et al. 2008). To address cellular mechanisms of accelerated retinal

damage, we assessed the effect of the strain on the loss of plasmalemma integrity in the retina by in vivo PI labeling. Figure 2b shows examples of PI fluorescence in the retina after in vivo administration. PI-positive cells were detected in the GCL and INL. Unexpectedly, RIP kinases and PI signals had different patterns of localization: PI signals were more common in INL, whereas signals of RIPKs were never detected. No significant difference in numbers of PI-positive cells was observed between old Wistar and OXYS rats (Fig. 2b), indicating equal presence of necrotic cells in both the affected by retinopathy retina and in a relatively healthy retina. This finding can also mean low sensitivity of the method for detection of necrosislike cellular injury. Besides, we observed an increase in the autofluorescence of RPE and erythrocytes after the administration of PI in vivo (Fig. 2f, g). This effect may be due to the greater permeability of the membranes of these cells to PI and a large amount of nucleic acids in them.

Increased amounts of Aβ deposits in the OXYS RPE or choroid

We next examined specificity of the $A\beta_{1–42}$ accumulation at the RPE–choroid interface by means of MOAB-2, a monoclonal antibody that detects several conformational species of $A\beta_{1–42}$ and does not detect amyloid precursor protein (APP). MOAB-2 is also selective for the more neurotoxic $A\beta_{1–42}$ compared to $A\beta_{1–40}$ (Youmans et al. 2012). Aβ-immunoreactive deposits were detected in perivascular macrophages of choroid in OXYS rats at 18 months of age. It is interesting that the double staining with the immune cell marker Iba1 barely revealed the joint localization of amyloid and Iba1-positive microglial cells in the choroid (Fig. 3).

Deleterious SNP in the *Pik3c2b* gene

We analyzed the genes related to autophagy for the presence of mutations (single-nucleotide polymorphisms, SNPs) in the OXYS rat's genome by means of previously obtained RNA-seq data (Telegina et al. 2015). Two synonymous and two nonsynonymous SNPs were found in the *Pik3c2b* gene associated with autophagy (Gene Ontology "macroautophagy", "autophagosome organization") (Table 1). One of the latter (located in exon 2) changes the tyrosine at position 288 to cysteine and was predicted to significantly affect protein structure or functions (scored as "deleterious") by the Variant Effect Predictor tool, VEP (SIFT algorithm) and had not been described in Ensemble (http://www.ensembl.org). Sanger sequencing in independent genomic OXYS DNA samples validated deleterious tAt/tGt SNP in the *Pik3c2b* gene. This SNP may be regarded as a novel molecular target for further studies aimed at assessing its role in the pathogenesis of AMD and accelerated aging in general.

Discussion

Here we revealed alterations in the amounts of autophagy proteins in the retina of senescence-accelerated OXYS rats, which spontaneously develop a retinopathy similar to AMD. Overall, our results indicate disturbances in the autophagy process in the retina of OXYS rats: its activation in the early stages of the disease and suppression in late stages. Several studies suggest that an autophagy decline or dysregulation is associated with AMD pathogenesis (Kaarniranta et al. 2013; Rodríguez-Muela et al. 2013; Mitter et al., 2014; Yao et al. 2015; Boya et al. 2016; Golestaneh et al. 2017). Hypoxia, oxidative stress, and parainflammation are pathogenic components of the AMD progression, and they are typical inducers of autophagy (Mitter et al. 2014; Ferrington et al. 2016; Kaarniranta et al. 2017). However, whether autophagy increases or declines with aging and disease remains controversial; the direction seems to depend on both the cell as well as the disease (Ferrington et al. 2016; Rodríguez-Muela et al. 2013).

The data from different model systems helped to formulate the valid hypothesis, i.e., that disruption of autophagy leads to retinal phenotypes associated with age-related degeneration (Rodríguez-Muela et al. 2013; Mitter et al., 2014; Yao et al. 2015; Boya et al. 2016; Golestaneh et al. 2017). Selective knockout in the RPE cells of autophagy inducer RB1CC1 results in age-dependent alterations of the RPE with formation of atrophic patches, subretinal migration of activated microglial cells, subRPE deposition of inflammatory and oxidatively damaged proteins, subretinal drusenoid deposits, and occasional foci of choroidal neovascularization (Yao et al. 2015). Recently it was demonstrated that RPE-specific

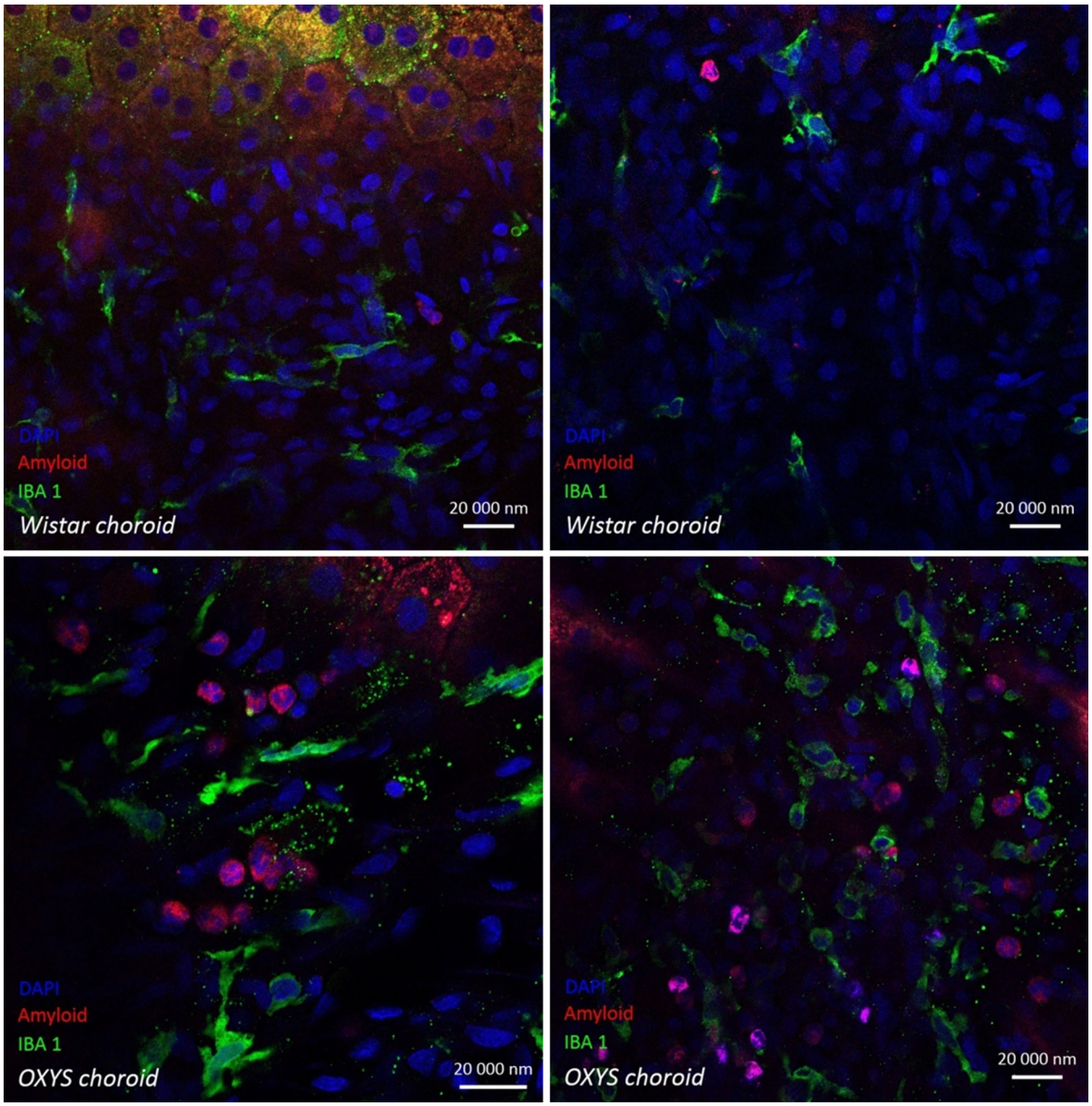

Fig. 3 Confocal images depict the choroid interface of 18-month-old Wistar (upper panel) and OXYS rats (low panel) with Aβ (Moab2) and Iba1 immunofluorescence. RPE set with the basal side up with the adjacent choroid. The level of Aβ fluorescence was higher in OXYS rats than in Wistar rats. Many perivascular macrophages in the aged choroid of OXYS rats contained Aβ deposits compared to the choroid of Wistar rats. Note that Iba1 signals marking microglial cells hardly colocalized with Aβ signals. Cell nuclei were stained with DAPI. Scale bar: 20 μm

deletion of Atg7 in mice leads to the signs of increased cellular stress such as hypertrophy and increased undigested cellular debris (Perusek et al. 2015). It can be assumed that alterations in the autophagy pathway in RPE somehow affect their cell size. Notably, significant RPE cell hypertrophy was observed in OXYS rats at 18 months of age during progressive stages of retinopathy (Telegina et al. 2017a, b). Taken together, these data provide evidence that downregulation of the autophagic pathway triggers degeneration of the RPE.

Table 1 SNPs in the *Pik3c2b* gene

Location (chr:pos)	CDS position	Protein position	Codon change	Amino acid change	SIFT (score)
13:49870101	863	288	tAt/tGt	Y/C	Deleterious (0.04)
13:49874587	1278	426	aaG/aaA	–	–
13:49905806	4398	1466	cgC/cgA	–	–
13:49905816	4408	1470	Act/Gct	T/A	Tolerated (1)

Results obtained in our research are in agreement with the notion that the character of changes in the process of autophagy depends on the stage of disease. Mitter et al. (2014) observed that the autophagic clearance system is significantly enhanced in two mouse models of early-onset AMD and in AMD patients' samples but it declines in late AMD. Furthermore, they found that downregulating the autophagic pathway renders the RPE more susceptible to oxidative stress, while increased autophagic flux protects the RPE from oxidative damage (Mitter et al. 2014).

Autophagic activity decreases with age, leading to a poor response to stress and inefficient clearance of damaged proteins in cells (Markaki and Tavernarakis 2011). The retinal Atg7 and Atg12 signals were stronger in aged Wistar rats than in OXYS rats, indicating the increase of the autophagy level during normal aging. We suggest that such increase in Wistar rats is adaptive and compensates for the age-related accumulation of aggregated proteins. In contrast, Rodriguez-Muela and colleagues reported a marked age-related reduction in macroautophagy in the mouse retina that was accompanied by a corresponding increase in chaperone-mediated autophagy (Rodríguez-Muela et al. 2013). Our study points to early exhaustion of the autophagy processes in the retina of OXYS rats, and this notion is consistent with their accelerated-senescence phenotype. A low efficiency of autophagy was detected in the kidneys of OXYS rats (Jankauskas et al. 2017). Furthermore, it can be uncompensated by chaperone-mediated proteolysis: previously, we reported a reduction of αB-crystallin (a small heat shock chaperone) expression in the retina of OXYS rats compared to Wistar rats (Muraleva et al. 2014).

Whether autophagic activity plays a harmful or a protective role in photoreceptor cell demise or rescue during responses to injury remains controversial (Xie et al. 2017). Depending on the cellular milieu, autophagy, as a lysosome-mediated self-degradation process of eukaryotic cells, can either promote survival or act as an alternative mechanism of programmed cell death for neurons. Anyway, an appropriate level of autophagic activity had a crucial positive influence on cell survival. It is believed that the prosurvival function of autophagy is achieved via its ability to block necrotic cell death (Shen and Codogno 2012). In our study, the level of autophagy was elevated at the early stage of retinopathy and declined at progressive stages. We can assume that the increase in autophagy leads to a moderate activity of apoptosis, indicated by the reduction of terminal deoxynucleotidyl transferase (TdT) dUTP nick-end labeled ($TUNEL^+$) cells at 3 months and changes in mRNA levels of genes associated with apoptosis (Telegina et al. 2015). By contrast, a decrease in autophagic activity level triggers necroptosis, as demonstrated by increased immunostaining of RIP-kinases. Recently Xie et al. (2017) showed that the augmentation of autophagy through TNF-α inhibition reduces apoptosis and enhances photoreceptor cell survival. Besirli et al. (2011) reported that inhibition of autophagy augments the expression of caspase 8 and increases the number of $TUNEL^+$ photoreceptor cells after retinal detachment, pointing to a protective effect of autophagic activity. In contrast, overactive autophagy may be cytotoxic (Hanus et al. 2013). Autophagy can promote cell death through excessive cellular autolysis, and by degrading fundamental cellular constituents (Wei et al. 2015). Apoptosis and necrosis seem to be activated flexibly depending on the cell type and cellular context in the retina (Trichonas et al. 2010). Hanus et al. (2013) demonstrated that necrosis, but not apoptosis, is a major type of cell death in RPE cells in response to oxidative stress. In our study, PI staining after in vivo administration and immunohistochemical staining of RIP-kinases has detected the

signs of necroptosis in the cells of an aged retina and RPE.

It is widely accepted that dysregulation of the autophagic process is associated with a detrimental accumulation of aggregated proteins. Autophagy controls the turnover of aggregate-prone proteins, such as amyloid, a process that is extremely important in post-mitotic cells, including the RPE (Kaarniranta et al. 2013; Ferrington et al. 2016). Previously, we found significant accumulation of $A_{1–42}$ in an aged OXYS retina by an ELISA and immunohistochemical analysis of cross-cryosections (Kozhevnikova et al. 2013b). Here we report Aβ accumulation (Moab2) in flat-mounted RPE/choroid of OXYS rats. Autophagy influences secretion of Aβ to the extracellular space; an autophagy deficiency induces aberrant intraneuronal Aβ accumulation in the perinuclear region leading to neurodegeneration (Nilsson et al. 2013).

A critical signaling lipid involved in the control of autophagy is phosphatidylinositol 3-phosphate (PI3P). Tight control of PI3P levels via coordination of phosphatidylinositol 3-kinases (PI3 Ks) and PI3P phosphatases is crucial for determining both the size and production rate of autophagosomes. In our study, we described a mutation exerting a possible deleterious effect on the structure and/or function of the protein encoded by the *Pik3c2* gene. *Pik3c2b* encodes a class II PI3 K (C2β isoform). Although Vps34 is the main PI3P source during autophagy, class II PI3 Ks also significantly contribute to PI3P generation and regulate autophagosome biogenesis (Devereaux et al. 2013). Recently, it has been revealed that depletion of class II PI3Ks reduces recruitment of WIPI-1 and LC3 to autophagosome nucleation sites and causes accumulation of the autophagy substrate p62 (Devereaux et al. 2013). PI3KC2β is a critical regulator of endosomal trafficking, specifically in insulin signaling, its inactivation potentiates insulin signals and sensitivity to insulin (Alliouachene et al. 2015). At present, we do not know the exact role of the uncovered deleterious SNP, but judging by PI3KC2β functions, we expect that it may affect PI3P levels and the architecture and dynamics of the enzyme complex. In addition to controlling autophagy, PI3P regulates endosomal traffic. In particular, PI3P regulates sorting and processing of APP and is selectively deficient in the brain tissue from humans with Alzheimer's disease and from relevant mouse models (Morel et al. 2013). We can hypothesize that a perturbation of PI3P metabolism may be a causative factor of AMD pathogenesis–related dysfunction of autophagy. Nonetheless, the contribution of the identified SNP and of the predicted deleterious effect to the development of the premature aging phenotype of OXYS rats has yet to be explored.

Conclusions

In summary, this study indicates that dysregulation of autophagy occurs during the development of AMD-like retinopathy in OXYS rats. Our results support the notion that autophagy can become a new therapeutic target for the development of drugs aimed at the prevention and treatment of AMD.

Acknowledgements Microscopy was performed at the Microscopy Center of the Institute of Cytology and Genetics, SB RAS, Russia. This work was supported by a Russian Scientific Foundation Grant (16-15-10005).

Compliance with ethical standards

Conflict of interest The authors declare that they have no conflicts of interest.

References

Alliouachene S, Bilanges B, Chicanne G, Anderson KE, Pearce W, Ali K, Scudamore CL (2015) Inactivation of the class II PI3K-C2β potentiates insulin signaling and sensitivity. Cell Rep 13(9):1881–1894. https://doi.org/10.1016/j.celrep.2015.10.052

Besirli CG, Chinskey ND, Zheng QD, Zacks DN (2011) Autophagy activation in the injured photoreceptor inhibits fas-mediated apoptosis. Invest Ophthalmol Vis Sci 52(7):4193–4199. https://doi.org/10.1167/iovs.10-7090

Boya P, Esteban-Martínez L, Serrano-Puebla A et al (2016) Autophagy in the eye: development, degeneration, and aging. Prog Retin Eye Res 55:206–245. https://doi.org/10.1016/j.preteyeres.2016.08.001

Devereaux K, Dall'Armi C, Alcazar-Roman A, Ogasawara Y, Zhou X, Wang F et al (2013) Regulation of mammalian autophagy by class II and III PI 3-kinases through PI3P synthesis. PLoS ONE 8(10):e76405. https://doi.org/10.1371/journal.pone.0076405

Dvoriantchikova G, Degterev A, Ivanov D (2014) Retinal ganglion cell (RGC) programmed necrosis contributes to ischemia–reperfusion-induced retinal damage. Exp Eye Res 123:1–7. https://doi.org/10.1016/j.exer.2014.04.009

Ferrington DA, Sinha D, Kaarniranta K (2016) Defects in retinal pigment epithelial cell proteolysis and the pathology associated with age-related macular degeneration. Prog

Retin Eye Res 51:69–89. https://doi.org/10.1016/j.preteyeres.2015.09.002

Golestaneh N, Chu Y, Xiao YY, Stoleru GL, Theos AC (2017) Dysfunctional autophagy in RPE, a contributing factor in age-related macular degeneration. Cell Death Dis 8(1):e2537. https://doi.org/10.1038/cddis.2016.453

Hanus J, Zhang H, Wang Z, Liu Q, Zhou Q, Wang S (2013) Induction of necrotic cell death by oxidative stress in retinal pigment epithelial cells. Cell Death Dis 4(12):e965. https://doi.org/10.1038/cddis.2013.478

Jankauskas SS, Pevzner IB, Andrianova NV, Zorova LD, Popkov VA, Silachev DN et al (2017) The age-associated loss of ischemic preconditioning in the kidney is accompanied by mitochondrial dysfunction, increased protein acetylation and decreased autophagy. Sci Rep 7:44430. https://doi.org/10.1038/srep44430

Kaarniranta K, Sinha D, Blasiak J, Kauppinen A, Veréb Z, Salminen A et al (2013) Autophagy and heterophagy dysregulation leads to retinal pigment epithelium dysfunction and development of age-related macular degeneration. Autophagy 9(7):973–984. https://doi.org/10.4161/auto.24546

Kaarniranta K, Tokarz P, Koskela A, Paterno J, Blasiak J (2017) Autophagy regulates death of retinal pigment epithelium cells in age-related macular degeneration. Cell Biol Toxicol 33(2):113–128. https://doi.org/10.1007/s10565-016-9371-8

Kolosova NG, Stefanova NA, Korbolina EE et al (2014) Senescence-accelerated OXYS rats: a genetic model of premature aging and age-related diseases. Adv Gerontol 4:294. https://doi.org/10.1134/S2079057014040146

Korbolina EE, Zhdankina AA, Fursova AZ et al (2016) Genes of susceptibility to early neurodegenerative changes in the rat retina and brain: analysis by means of congenic strains. BMC Genet 17(Suppl 3):153. https://doi.org/10.1186/s12863-016-0461-7

Kozhevnikova OS, Korbolina EE, Ershov NI, Kolosova NG (2013a) Rat retinal transcriptome: effects of aging and AMD-like retinopathy. Cell Cycle 12(11):1745–1761. https://doi.org/10.4161/cc.24825

Kozhevnikova OS, Korbolina EE, Stefanova NA et al (2013b) Association of AMD-like retinopathy development with an Alzheimer's disease metabolic pathway in OXYS rats. Biogerontology 14(6):753–762. https://doi.org/10.1007/s10522-013-9439-2

Lim LS, Mitchell P, Seddon JM, Holz FG, Wong TY (2012) Age-related macular degeneration. Lancet 379(9827):1728–1738. https://doi.org/10.1016/S0140-6736(12)60282-7

Markaki M, Tavernarakis N (2011) The role of autophagy in genetic pathways influencing ageing. Biogerontology 12(5):377–386. https://doi.org/10.1007/s10522-011-9324-9

Mitter SK, Song C, Qi X, Mao H et al (2014) Dysregulated autophagy in the RPE is associated with increased susceptibility to oxidative stress and AMD. Autophagy 10(11):1989–2005. https://doi.org/10.4161/auto.36184

Morel E, Chamoun Z, Lasiecka ZM, Chan RB, Williamson RL, Vetanovetz C et al (2013) PI3P regulates sorting and processing of amyloid precursor protein through the endosomal system. Nat Commun 4:2250. https://doi.org/10.1038/ncomms3250

Muraleva NA, Kozhevnikova OS, Zhdankina AA et al (2014) The mitochondria-targeted antioxidant SkQ1 restores αB-crystallin expression and protects against AMD-like retinopathy in OXYS rats. Cell Cycle 13(22):3499–3505. https://doi.org/10.4161/15384101.2014.958393

Nilsson P, Loganathan K, Sekiguchi M, Matsuba Y, Hui K, Tsubuki S et al (2013) Aβ secretion and plaque formation depend on autophagy. Cell Rep 5(1):61–69. https://doi.org/10.1016/j.celrep.2013.08.042

Perusek L, Sahu B, Parmar T, Maeno H, Arai E, Le YZ et al (2015) A2E Accumulation and the Maintenance of the Visual Cycle are Independent of Atg7-mediated Autophagy in the Retinal Pigmented Epithelium. J Biol Chem 290(48):29035–29044. https://doi.org/10.1074/jbc.M115.682310

Rodríguez-Muela N, Koga H, García-Ledo L, de la Villa P, de la Rosa EJ, Cuervo AM, Boya P (2013) Balance between autophagic pathways preserves retinal homeostasis. Aging Cell 12(3):478–488. https://doi.org/10.1111/acel.12072

Shen HM, Codogno P (2012) Autophagy is a survival force via suppression of necrotic cell death. Exp Cell Res 318(11):1304–1308. https://doi.org/10.1016/j.yexcr.2012.02.006

Stefanova NA, Kozhevnikova OS, Vitovtov AO et al (2014) Senescence-accelerated OXYS rats: a model of age-related cognitive decline with relevance to abnormalities in Alzheimer disease. Cell Cycle 13(6):898–909. https://doi.org/10.4161/cc.28255

Telegina DV, Korbolina EE, Ershov NI, Kolosova NG, Kozhevnikova OS (2015) Identification of functional networks associated with cell death in the retina of OXYS rats during the development of retinopathy. Cell Cycle 14(22):3544–3556. https://doi.org/10.1080/15384101.2015.1080399

Telegina DV, Kozhevnikova OS, Bayborodin SI, Kolosova NG (2017a) Contributions of age-related alterations of the retinal pigment epithelium and of glia to the AMD-like pathology in OXYS rats. Sci Rep 7:41533. https://doi.org/10.1038/srep41533

Telegina DV, Kozhevnikova OS, Kolosova NG (2017b) Molecular mechanisms of cell death in retina during development of age-related macular degeneration. Adv Gerontol 7:17. https://doi.org/10.1134/S2079057017010155

Trichonas G, Murakami Y, Thanos A et al (2010) Receptor interacting protein kinases mediate retinal detachment-induced photoreceptor necrosis and compensate for inhibition of apoptosis. Proc Natl Acad Sci USA 107(50):21695–21700. https://doi.org/10.1073/pnas.1009179107

Unal Cevik I, Dalkara T (2003) Intravenously administered propidium iodide labels necrotic cells in the intact mouse brain after injury. Cell Death Differ 10(8):928–929. https://doi.org/10.1038/sj.cdd.4401250

Wei T, Kang Q, Ma B, Gao S, Li X, Liu Y (2015) Activation of autophagy and paraptosis in retinal ganglion cells after retinal ischemia and reperfusion injury in rats. Exp Ther Med 9(2):476–482. https://doi.org/10.3892/etm.2014.2084

Xie J, Zhu R, Peng Y, Gao W, Du J, Zhao L et al (2017) Tumor necrosis factor-alpha regulates photoreceptor cell autophagy after retinal detachment. Sci Rep 7(1):17108. https://doi.org/10.1038/s41598-017-17400-3

Yao J, Jia L, Khan N, Lin C, Mitter SK, Boulton ME, Dunaief JL, Klionsky DJ, Guan J-L, Thompson DA, Zacks DN (2015) Deletion of autophagy inducer RB1CC1 results in degeneration of the retinal pigment epithelium. Autophagy 11(6):939–953. https://doi.org/10.1080/15548627.2015.1041699

You Z, Savitz SI, Yang J, Degterev A, Yuan J, Cuny GD et al (2008) Necrostatin-1 reduces histopathology and improves functional outcome after controlled cortical impact in mice. J Cereb Blood Flow Metab 28(9):1564–1573. https://doi.org/10.1038/jcbfm.2008.44

Youmans KL, Tai LM, Kanekiyo T et al (2012) Intraneuronal Aβ detection in 5xFAD mice by a new Aβ-specific antibody. Mol Neurodegener 7:8. https://doi.org/10.1186/1750-1326-7-8

Zhang J, Bai Y, Huang L, Qi Y et al (2015) Protective effect of autophagy on human retinal pigment epithelial cells against lipofuscin fluorophore A2E: implications for age-related macular degeneration. Cell Death Dis 12(6):e1972. https://doi.org/10.1038/cddis.2015.330